Nuclear Inst. and Methods in Physics Research, A 1048 (2023) 167919

Contents lists available at ScienceDirect

Nuclear Inst. and Methods in Physics Research, A

journal homepage: www.elsevier.com/locate/nima

# The GISANS instrument at the HBS

Sebastian Jaksch [a,b], Klaus Lieutenant [c], Earl Babcock [a], Henrich Frielinghaus [a,*]

[a] Forschungszentrum Jülich GmbH, Jülich Centre for Neutron Scattering JCNS-4 at MLZ, Lichtenbergstrasse 1, 85747 Garching, Germany
[b] Technische Universität München, Heinz Maier-Leibnitz Zentrum (MLZ), Lichtenbergstrasse 1, 85747 Garching, Germany
[c] Forschungszentrum Jülich GmbH, Jülich Centre for Neutron Scattering JCNS-2, Wilhelm Johnen Strasse, 52425 Jülich, Germany

ARTICLE INFO

*Keywords:*
Grazing incidence small-angle neutron scattering
Neutron reflectometry
Pulsed source
Instrumentation
Ray-tracing computer simulations

ABSTRACT

This manuscript describes a concept of a grazing incidence small-angle neutron scattering (GISANS) instrument for the high brilliance source (HBS). The HBS being a compact pulsed neutron source using a moderate energy proton accelerator which allows for very compact moderators and shielding, and flexible pulse repetition rates. Similar to many other instrument concepts for this source, the lowest proposed HBS pulse frequency of 24 Hz with a relatively large detector distance is the optimal choice for the instrument described here in terms of obtained intensity and Q-range (i.e. scattering vector range). Such a configuration has the added advantage of good Q-resolution, which is important when scattering depths need to be resolved well. This is especially the case for GISANS when the incident angle is close to the critical angle of total reflection. The performance obtained from detailed ray-tracing computer simulations predict a high performance instrument that will be comparable to reflectometers and small angle neutron scattering (SANS) instruments at high-flux reactor sources such as the Forschungsreaktor Munich (FRM-2) and others.

## 1. Introduction

Neutrons for scattering experiments can be produced in several different ways [1]. There are the traditionally used fission research reactors that produce neutrons continuously. Inside the room temperature reactor core thermal neutrons hit $^{235}$U nuclei that then decay to several lighter elements and release approx. 2.5 neutrons that either reenter the nuclear reaction or leave the reactor, often after moderation to a colder temperature, as the desired neutron beam. Another method is spallation neutron sources which utilize high-energy protons of 0.5 to 3 GeV (typically 1.3 GeV) impinging on a heavy metal target for example tungsten for the European Spallation Source, ESS, in Lund Sweden [2] and for ISIS (the Egyptian goddess gave the name for this neutron source) at the Rutherford Appleton Laboratory in U.K. or liquid mercury for the Spallation Neutron Source, SNS in USA to cause these heavy nuclei to decay into lighter elements typically releasing 20–30 neutrons per nucleus. From the nature of the proton accelerators and the history of their development, the beam tended to be pulsed at the AC line frequency of 60 Hz at the SNS, 50 Hz at ISIS and $\frac{1}{2}$ AC line frequency of 25 Hz at J-Parc, whereas the recently designed ESS takes into account new accelerator technology and the idea of a highly coupled moderator to use a 14 Hz frequency, or ISIS T2 which now takes 1 out of 5 proton pulses of the ISIS proton accelerator to produce a 10 Hz from its target. Consequently the neutrons appear in bundles grouped in time occurring at the frequency of the particular source. Each neutron pulse contains a Maxwellian, or Maxwellian-like distribution of velocities that can be distinguished at the position of the neutron instrument's detectors that are placed a certain distance from the moderator by measuring the so-called time-of-flight of the neutrons between the two (in modern cold sources the neutrons are not completely equilibrated such that the actual temperature is lower than that of the neutron spectrum [3,4] and several Maxwellian distributions need to be used to describe the neutron spectrum of a realistic cold source [5,6]). Both the source frequency and source-moderator details lead to different optimal instrument parameters and types of instruments for each source. A revolutionary concept was introduced by the low-energy high-brilliance neutron sources [7,8] to modify this former paradigm. These sources accelerate protons rather only to moderate energies (typically 70 MeV) in order to utilize lighter element targets (Tantalum in the HBS) at a more flexible frequency that can be multiplied depending on the properties of the desired neutron beam (24 Hz and multiples for the HBS). The central idea of the HBS is to increase the efficiency of production of the most desirable (moderated) neutrons with high brilliance by suppressing unwanted background containing other particles and neutrons. Here brilliance is similar to that in light optics, a flux per unit solid angle, and can be used as a figure of merit as defined by Ref. [8]. The HBS should be seen as a progression of a series of Compact lower energy Accelerator-driven Neutron Sources (CANS) around the world, where examples are LENS [9], CPHS [10], HUNS [11] and RANS [12]. However these sources are typically university based neutron sources

* Corresponding author.
*E-mail address:* h.frielinghaus@fz-juelich.de (H. Frielinghaus).

https://doi.org/10.1016/j.nima.2022.167919
Received 31 July 2022; Received in revised form 13 December 2022; Accepted 13 December 2022
Available online 17 December 2022

for education and have associated limitations for operations and the development of large scale neutron instrumentation which is normally undertaken at the larger national and international centers described in the beginning of this section. Essentially neutron sources focused on scattering methods for materials science rely on cold sources [4,13] that cool the neutron energy distributions down to so-called "cold" Maxwellian spectrums i.e. with a characteristic temperature of 20–30 K which corresponds to a peak neutron wavelength of around 0.4 nm (the actual spectrum is a superposition of three Maxwellian distributions as discussed above [4,5]). This wavelength band is useful for nanometer length scale investigations which is the size scale of interest to common GISANS, the target of the instrument described here. For more details we refer to the cited literature [14–16].

The development of the Jülich High Brilliance Source (HBS) [7,8] is currently at the stage of a technical design report in terms of the source development and instrumentation concepts. It is envisioned to be able to use different neutron pulse schemes simultaneously by utilizing multiple target stations with different frequencies and moderator geometry specifically optimized for groups of instruments. The present design has 3 target stations with frequencies of 24 or 96 Hz foreseen which would have pulse lengths defined by the 1.6% duty cycle of the specified proton accelerator. Each of the three target-moderator-reflector units are optimized for the resulting pulse lengths. Here, due to the high brilliance of the small target-moderator assemblies the addition of neutron reflectors help further increase the flux and brightness of desired neutrons for instrumentation. The resulting design allows for essentially 1D cold moderator that can be engineered individually for each instrument much like an instrument component. In other words, because of the small moderator dimension each target station can contain several individually optimized moderators.

The configuration optimal for large scale structure instruments on pulsed broadband sources usually tends towards slower frequencies and the use of a broader wavelength band. In the simplest case the total instrument length determines the TOF resolution, which in turn determines the wavelength (and therefore the Q-) resolution [17]. The long pulse source ESS is conceptionally different because it uses choppers to determine the neutron pulse time-width rather than the source pulse itself [14]. This time structure lends itself well to large scale structure instruments as it actually leads to shorter optimal instrument lengths which are more economical to build. The authors have also designed instruments and neutron optics for the ESS source for different applications than those presented here [17–22]. While differing in both the neutron pulse structure and applications, the methods and principles used for instrument optimization and design are in common with the instrument presented here.

The method of grazing incidence (small-angle) (neutron) scattering [23,24] was developed for characterizing near-surface structures using classical scattering instruments by impinging beams under grazing incidences onto planar samples. If the incident angle, $\alpha_i$, (see Fig. 1) is below the critical angle of total reflection, $\alpha_c$, an evanescent wave develops that tunnels inside the sample. The resulting scattering patterning will emphasize the near surface structure of the sample characterized by a tunneling or so-called scattering depth, $\Lambda$, which becomes the length scale accessible to such investigations [25]. Additionally, special surface-modes are excited by the (x-ray or neutron) radiation for impinging angles close to and above the critical angle providing another enhancement [26]. For example, the Yoneda peak displays at a characteristic exit angle, $\alpha_f$, (e.g. Yoneda angle) and contains the surface structure information for the horizontal line cut through the Yoneda peak along $\theta_f$ (i.e. in the lateral direction, see Fig. 1). For layered materials with strong diffraction at multiple interfaces [27] the (x-ray and neutron) wave fields are usually more complicated and the highlighted regions need to be analyzed in more detail. With diligence to perform the appropriate analysis GISANS experiments reveal valuable depth-resolved structural information that often is buried inside layered materials [28]. Neutrons have the huge advantage of centimeter scale penetration depths that makes them ideally suited to study solid–liquid interfaces.

For GISANS measurements, a slightly modified standard small-angle neutron scattering (SANS) instrument can be used to accommodate the technical needs [17]. The entrance aperture can be a slit with a narrow dimension in the normal direction and the standard SANS dimension in the lateral dimension. The normal direction is perpendicular to the sample interface or layering, and the lateral direction in its/their plane. The sample aperture usually confines the beam in the lateral direction, and the footprint of the sample confines the beam in the normal direction, but also here the aperture might limit the beam. The sample is mounted on a cradle to allow an adjustment of the lateral direction with the apertures and for varying the incident angle for reflectometry scans or GISANS measurements.

Opposed to the simple transmission geometry of a normal SANS sample, GISANS measurements of solid samples often mount the sample on a wafer for support. The GISANS pattern in the "upper" hemisphere is usually kept open and the sample-wafer surface leaves an air or vacuum path for the scattered neutrons reflected from its surface. To observe the GISANS pattern of the neutron refracted into the sample-wafer, i.e. in transmission appearing in the "lower" hemisphere of the scattering pattern, the other side of the sample-wafer must also be kept free for propagating neutrons. For solid–liquid interfaces often a silicon slab is used to cover the "upper" hemisphere. The neutrons impinge the slab first on the vertical side where neutron refraction is negligible, then hit the solid–liquid interface where considerable refraction takes place, interact with the sample, reflect back into the slab and then leave it on the second downstream vertical side — again without considerable refraction. Additionally constructions for observing the "lower" hemisphere of a solid–liquid interface to measure the sample-transmitted neutrons have been proposed [29]. Normally classical SANS instruments do no elevate their detectors (REFSANS however is a counter example, which does employ elevation of the detector [30]). In GISANS, the small critical angles of total reflection (e.g. 0.5° for the silicon-$D_2O$ interface at 8 Å wavelength) and the commonly used detector distances of 8 m or less for most applications do not strictly require an elevation of the detector given the large detector size employed on such SANS instruments.

Another often proposed GISANS option uses finer collimation in the sample-perpendicular direction to increase resolution the lateral direction. This is done by closing the entrance aperture to similar dimensions in either direction to create a so called "pencil-collimation" where we note that the vertical aperture is naturally limited by the sample length to a relatively small dimension as in reflectometry. Therefore this pencil collimation reduces the available intensity dramatically, however the increase in resolution in the lateral direction allows for observing quite small $Q_y$ [24] (i.e. the scattering vector in the lateral direction, orthogonal to $Q_z$ in the normal direction — see Fig. 1).

Currently 3 SANS instruments are considered for HBS where only the one described here is planned to have a GISANS option. Clearly such an instrument can also be operated as a classical SANS instrument and in this mode the same performance as the proposed high-throughput SANS instrument would be obtained due to the similar "front-end" requirements of the two instruments. For GISANS measurements the highest possible flux is required because a slit geometry is used (i.e. smaller vertical apertures than for SANS) and the resulting scattering volume is small. Consequently a large sample is normally also beneficial for the experiment. Other enhancement effects, such as the use of evanescent waves or a possible resonator [25,27,31–35], may also be used to increase the scattered intensity, however the acquisition times per sample normally remain longer for GISANS measurements than for classical SANS, due to both the geometric limitations of sample-length and fundamental interaction volume from the scattering depth $\Lambda$. In this sense, the neutron extraction and guide systems must be optimized for flux.

A second point for the design of a GISANS instrument is one should have the ability to measure the reflectivity curve at the beginning of

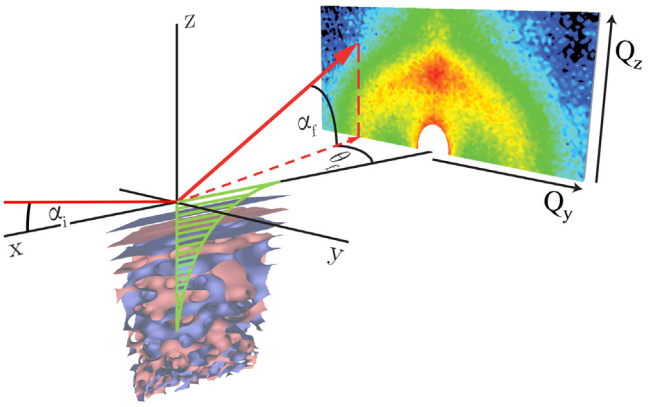


**Fig. 1.** Sketch of the GISANS geometry with neutron path (red line), a microemulsion in the lower hemisphere, an indicated evanescent wave (green), and an detector image with the two scattering vector components ($Q_y$, $Q_z$) in the lateral and normal direction.

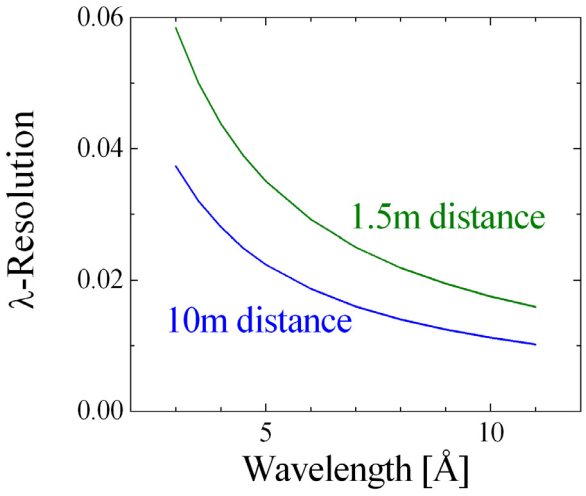


**Fig. 2.** The wavelength resolution of the 10 + 10 m SANS instrument at the 24 Hz source from geometric considerations. The formula reads: $\lambda$-Resolution(relative units) = $\Delta$t [ms]/(3.956 $\lambda$ [Å] L [m]) with the pulse length $\Delta$t = 0.67 ms, the wavelength $\lambda$, and the detector distance L from the source (13.55 + 1.5 m or 13.55 + 10 m).

each experiment, so the instrument should also have a mode like a classical reflectometer [16,36]. This verifies that the sample-substrate structure is correct, and also allows initial observation of certain parameters of the sample structure. Furthermore, this part of the experiment characterizes which regions of the sample are highlighted as a function of the incident angle. Only after determining the reflectivity curve to characterize the in-plane sample structure, can the instrument be switched to the GISANS mode to observe the details of the lateral structure.

## 2. Science case

Recent reviews discuss the many-fold applications of the GISA(N)S method in detail [37–40] (we refer here to grazing incidence small angle scattering in general because often x-rays are also employed). The science case of GISANS instruments is supported by but not limited to several recent examples such as: lipid bilayers [41] (be it supported from a substrate or at the air–liquid interface), membranes for fuel cells [42] or reverse osmosis [43], lithium batteries [44], thin skyrmion layers [45], spray deposition of organic solar cells [46], and cellulose fibrils (for sensors) [47].

To emphasizing a particular example, the air–liquid interface of certain surface-active substances can be studied close to or above the critical micelle concentration (which usually means low concentrations, i.e. low scattering intensities) [48]. Another important aspect of neutrons for the study of solid–liquid interfaces is that only neutrons can penetrate centimeters of certain types of relevant substrates [31]. Here, many important chemical processes can be uniquely investigated such as electrochemical processes (batteries, [44]) and catalysis because of this neutron penetration for instance [42]. As perhaps implicitly indicated, to study such chemical processes in focus, requires short acquisition times to resolve their kinetics. Another applied aspect of kinetic measurements is the spray deposition of various materials where the drying and vapor exposure over time are key. All these proposed topics focus on structural sizes between a few nanometers to a few 100 nanometers in both (lateral and normal) directions. Thus, the classical method SANS only needs to be modified a little. Where the aspects of classical neutron reflectometry limit the structural sizes observed in the normal directions to a few 10 nanometers, the scattering depths in a GISANS experiment easily overcome this limit and may even reach out for micrometers as discussed below.

## 3. Instrumental demands

We present several of the basic requirements/specifications of the GISANS instrument and the reasoning influencing the chosen parameters. First, measurement of reflectivity normally limited to a $Q_{z,max}$ = 0.2 Å$^{-1}$. This value is chosen because at the maximum $Q_z$, the classical Fresnel reflectivity of $10^{-6}$ to $10^{-7}$ compares well to expected instrumental background, and therefore only layered structures with Bragg peaks display observable intensities after this Q_z. Practically, most GISANS applications stop here and, for resolving Bragg peaks, a dedicated reflectometer is used instead. Second a high scattering depth resolution for observing near surface structures is desired. Third, a standard SANS resolution and range is desired, for example $Q_y$ = 0.002 to 1.8 Å$^{-1}$ (for this time-of-flight GISANS instrument the values are to be understood as rather typical values rather than the extreme limits). And finally it is clear that for highest intensities, if the integrated intensity is simply proportional to area, large samples of sizes of typically 2 to 5 cm wide by 15 cm long are used and it will be necessary to illuminate them fully.

It turns out that the scattering depth resolution is tightly connected to the wavelength resolution, which is shown in Fig. 2, because the slit geometry (typical for reflectometry experiments with small dimensions in the normal direction and wider dimensions in the lateral direction) strongly suppresses divergence effects in the normal direction. Therefore to achieve a high wavelength resolution a long instrument is chosen, in this case 10 + 10 m for the collimation and detector distance. The resulting time distance plot for the preferred 24 Hz source is depicted in Fig. 3. In this case the $Q_y$ resolution is obtained naturally because is related to classical SANS dimensions. Conversely the $Q_{z,max}$ demands for a large divergence in the vertical direction delivered to the entrance apertures if we want to cover many incident angles simultaneously. Using neutron mirrors, several distinct beams can be directed to the sample. For further intensity enhancement in the GISANS mode, resonators may be embedded in the substrate. Because many experiments aim at thin magnetic layers or incoherent hydrogen scattering suppression, polarization and polarization analysis is also highly recommended for the GISANS instrument. As the instrument is long, the implementation of polarization is straightforward and can easily be accomplished via removable transmission super-mirrors perhaps as a V-cavity so that the beam divergence and direction are not modified by the polarization option [49]. The polarization initially is in the vertical direction and may be adiabatically turned by 90° within the collimation.

## 4. Depth resolution

The scattering depth $\Lambda$ normalized to $\Lambda_0$, the scattering depth at zero incidence angle, as a function of the critical angle normalized

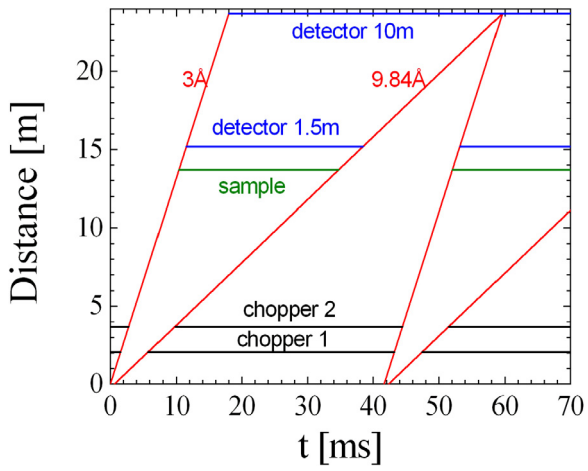


**Fig. 3.** Time distance plot of the GISANS instrument with a usable bandwidth of 6.8 Å at the 24 Hz source. The choppers, the sample, and the 2 detectors are indicated.

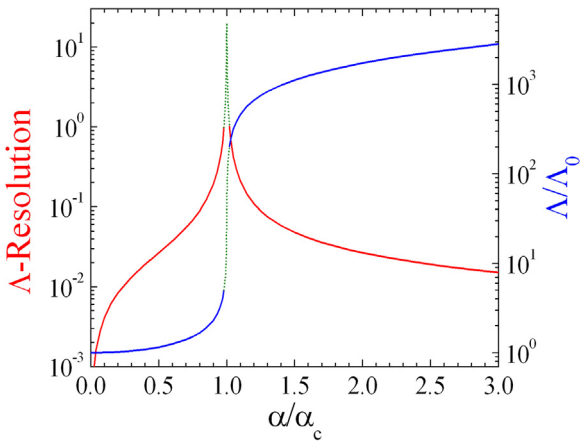


**Fig. 4.** Resolution scheme of the evanescent wave to study the structure in the normal direction. The scattering depth $\lambda$ (blue curve) switches between evanescent wave and damped wave through sample scattering. The derivative determines the resolution of the depth-resolved GISANS measurement (red curve). The green dotted continuations of the two curves (blue and red) indicate the forbidden range, where the instrumental resolution is insufficient.

incidence angle, ($\alpha/\alpha_c$), is depicted in Fig. 4, blue curve. Below the critical angle, the evanescent wave determines the irradiated depth. As can be seen the range of the accessible scattering depths varies between 200 (= $\Lambda_0$) and 2000 Å, i.e. $1 \leq \Lambda/\Lambda_0 \leq 10$. The smallest incident angles are not accessible because the footprint becomes very small and the GISANS scattering intensity vanishes. We note that the scattering depth at zero incidence angle $\Lambda_0$ can be shifted by changing the overall averaged scattering length density of the sample [50] to modify the absolute scale of this curve. The change of scattering length density is connected to the contrast of the scattering experiment and is often applied for SANS experiments [51,52] in order to highlight specific features of the sample structure (usually by exchanging hydrogen by deuterium). However, when rendering the scattering depth larger, a smaller scattering length density difference between the reference material through which the radiation impinges and the overall sample is needed. Above the critical angle, the left hand portion of the plot in Fig. 4, the scattering depth is dominated by absorption, and strong small angle and incoherent scattering [28,53]. The depicted curve corresponds to a strongly scattering sample case where many neutrons are taken from the primary intensity, specifically with a total absorption/scattering probability of $\Sigma_{tot} = 6\ cm^{-1}$, which is realistic for microemulsion samples. For weaker scattering samples the corresponding plateau can lie orders of magnitudes higher and even larger size structures are accessible approaching the μm scale. The derivative of this curve determines the depth resolution of a GISANS experiment (red curve). In this case the depth resolution is shifted by the wavelength resolution, and it lies rather low for this long GISANS instrument. The typical depth resolution for small incident angles lies in 2% range, but at the critical angle of total reflection the value can exceed 100% and the gathered scattering information becomes useless. So a gap for the resolved depths opens up. In the considered example, a single order of magnitude is inaccessible. But it can be also several orders of magnitude. So a very good wavelength resolution is highly recommended for depths of up to a few 1000 Å. The range of the high scattering depths remains an issue to the absorption/scattering probability of the sample which cannot always be chosen purposely. Angles above the critical angle of total reflection remain an issue to a diligent analysis of all absorption/scattering contributions with their specific wavelength dependence (absorption $\Sigma_{abs} \sim \lambda^1$, small angle scattering $\Sigma_{sans} \sim \lambda^2$, incoherent scattering $\Sigma_{inc} \sim \lambda^0$).

## 5. Layout

The layout of the instrument is based on the demand of $Q_z$ for air–liquid interfaces (Fig. 5). The first idea was to incline the beamline down by about 1 deg. However, several inclination angles are needed to cover the wanted Q-range in one reflectivity measurement and we can only use the down-directed neutrons for the smallest incident angle without mirrors. Whereas with sufficient vertical divergence in the incoming beam we can reach higher inclination angles by mirrors (see Fig. 5). We chose distinct incidence angles of 0.4°, 1° and 2.5° (that reach up to $Q_z = 0.2\ Å^{-1}$ with wavelengths from 3 to 9.8 Å), and fully cover incident angles below and above the critical angle of total reflection for common samples. Note that the critical angle between silicon and $D_2O$ is 0.5° for 8 Å neutrons for example. For the lowest incidence angle of 0.4°, the whole instrument may be tilted upwards by 0.65° and the upper and lower mirrors of the guides will need to have an m-value of 3.85 (the relative critical angle $\alpha_c$ of total reflection versus Ni, $\alpha_c = 0.1°\ m\ \lambda\ [Å]$) to accommodate this inclination. The reflectivity measurements will be conducted with a collimation distance of 4 m, and two mirrors reflect the rays with incidence angle of 1° and 2.5°. Then the three different beams can be well separated and detected simultaneously at a detector distance of 4 m. This option is only used for reflectivity measurements when the off-specular scattering is weak and it does not disturb the specular intensities as a background source. For GISANS measurements, the collimation can be rendered between 10 m and 2 m distance and only a single beam is used (all mirrors are taken out) where collimations between 4 m to 10 m are expected to be the most commonly used based on experience (and the 2 m is reserved for classical SANS experiments). The sample is then in the center of the collimated beam, and the incident angle can be changed by turning the sample. Except for air–liquid interfaces which must remain horizontal so for these samples the incident angle is chosen by the height of the sample with respect to the collimation aperture, i.e the beam collimation itself is used to tune the incident angle and therefore the angles will be limited by the total beam height. The detector tube is connected to an arm virtually anchored at the sample position and can be tilted between 0° and 5° in the vertical direction. Two 1 $m^2$ detectors will be used, a movable one positioned between 1 and 4 m and a fixed position one at 10 m. The beam extraction from the source which will be 3 cm diameter is performed by a deflector that shifts the beam by 4 cm horizontally. Using the 2 × 2 $cm^2$ cross section of all guides, this corresponds to a line out of sight by a factor of 2. The choppers are placed at 2.05 m and 3.68 m which leaves enough space for the polarizer between them. The whole extraction concept corresponds to the previously optimized high-throughput SANS but here with the inclination ensuring an optimal divergence transport to

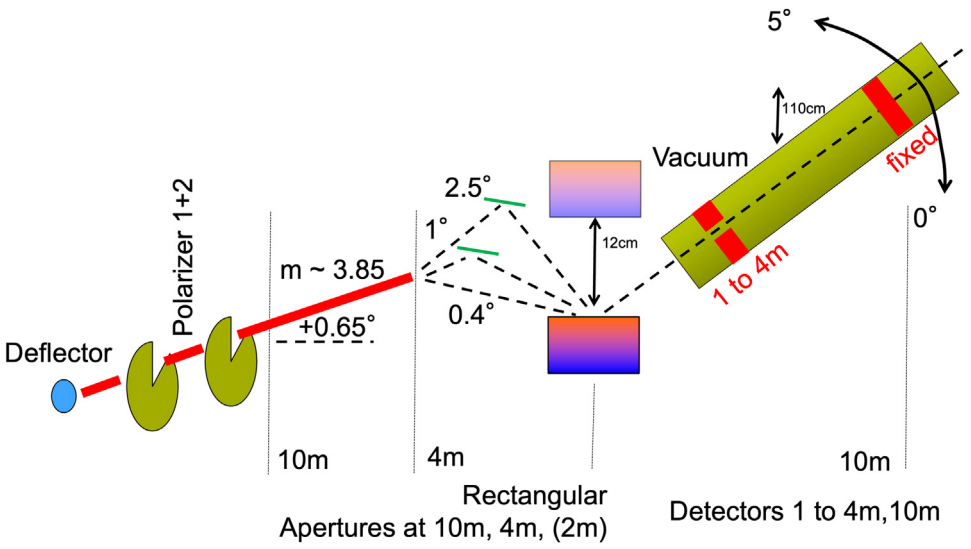


**Fig. 5.** Scheme of the GISANS instrument with an inclination of 0.65° and m = 3.85 for the vertical direction to cover the distinct rays at angles of 0.4°, 1° and 2.5° in the reflectometry mode for the air–liquid interface (as shown here). Several incident angles are selected to observe the specular reflectivity simultaneously at a wide range. The detector tube can be tilted between 0° and 5° in the vertical direction. The incident angles of 1° and 2.5° are exaggerated and the reflected beams can well be collected at a detector distance of 4 m.

the sample. The sample space can be of the approximate size of 2 × 2 m.

To refine and verify this instrument concept McStats neutron ray-tracing computer simulations were used [5,6]. We model the beams reflected to a virtual high-resolution detector at 4 m distance with an active area of 75 × 75 cm$^2$ is depicted in Fig. 6 cm$^2$ for demonstrating the reflectometer mode whereas the proposed detector will be a 1 × 1 m$^2$ size. One can see the reflected beams of the upper hemisphere, and the transmitted beams in the lower hemisphere. The distinct beams correspond to incidence angles of 0.4°, 1° and 2.5° occurring at $Q_z$ = 0.02, 0.05, and 0.14 in the plot, also shown is a 4° incident angle which is at $Q_z = 0.2$ Å$^{-1}$ for the respective $Q_z$ values of the specular reflection for a given neutron wavelength of 4 Å (as the representative for the band 3 to 9.8 Å). Whereas described earlier we select several incidence angles in order to observe the specular reflectivity simultaneously over a wide $Q_z$ range. The corresponding mirrors need to be coated with m-values of 4, 4, 7 and 9 respectively. The last value of m = 9 indicates that the highest possible angle remains to be achieved by current technology due to this high m (a similar high m is also recommended for the reflectometer HERITAGE [15]) whereas current technology is limited to around m = 7 [54] or m = 8 [55]. Additionally, the option of a fourth mirror while increasing the $Q_z$ would disproportionately decrease available sample space due to its physical location near the sample, a fourth mirror with m = 9 would reduce the sample space by approx. 60 cm along the neutron flight path (a similar reduction is expected for an adaption of the design for m = 8). Consequently, the three-beam option seems to be more reasonable and currently feasible. An important feature of the three beams is the adapted resolution that relaxes with higher angles due to the larger footprint of the mirrors. Currently, the simulations are based on planar mirrors and so the collected intensities are relatively weak especially at the 2.5° angle. Focusing mirrors (i.e. 1-dim elliptical in shape) could be used to increase the collected intensities for the three beams by 25% by changing the intensity profile at the sample along the $x$-axis from triangular over-illuminating spot (with the wings missing the sample) a to rectangular sample-size matched spot as is the case for most focusing optics [56].

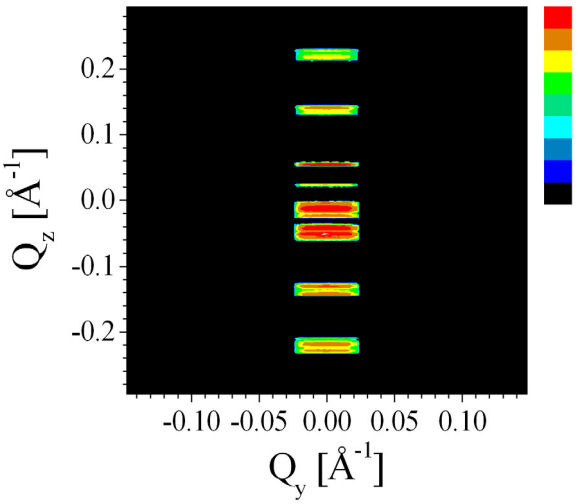


**Fig. 6.** The reflected and transmitted beams from the mirrors at incidence angles of 0.4°, 1°, 2.5° (and 4°) in reflectometry mode. The upper hemisphere depicts the reflected beams, and the lower hemisphere the bypassing beams. The intensity scale is logarithmic.

## 6. Performance

To gauge the performance of this instrument a GISANS image for the 10 m detector is simulated for a microemulsion at a relatively high incident angle of 1° (Fig. 7). The simulated intensities of this instrument refer to the standard collimation of 2 m in the SANS mode and using a hydrogen moderator on a 24 Hz target. 1.8 to 2.2 × 10$^8$ n/cm$^2$/s are to be expected from the McStas simulations with the wavelength resolution depicted in Fig. 2 and a 2 × 2 cm$^2$ collimation. The 2 m collimation is used as a benchmark for all SANS instruments worldwide because this is where the flux is usually highest, even though the instruments typically operate at larger collimation distances for higher resolution and lower flux. The simulated fluxes rely on the code of the HBS cold source provided by the author KL and were double checked with the simulation package VITESS as well. A detailed simulation of the neutron spectrum at the sample position for this instrument is displayed in Fig. 8 (for the sample being in the center of the beam). Here, we see the absolute brilliance as a function of wavelength. The peak brilliance is obtained around the wavelength of 4 Å and the typical decay towards higher wavelengths occurs due to the Maxwell

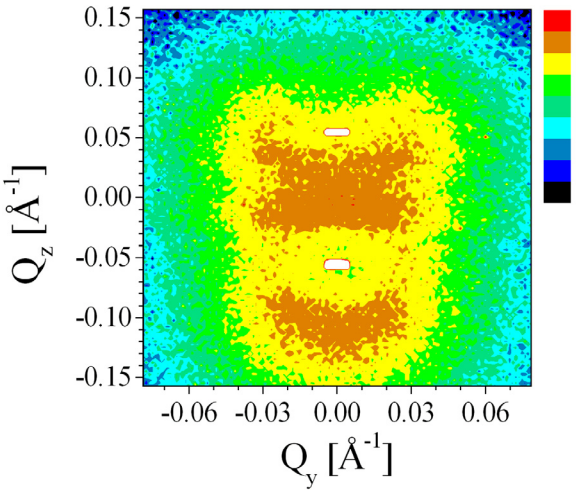


**Fig. 7.** A simulated GISANS image on the 10 m detector of a microemulsion for relatively high incident angles of 1° with a white beam. The intensity scale is logarithmic.

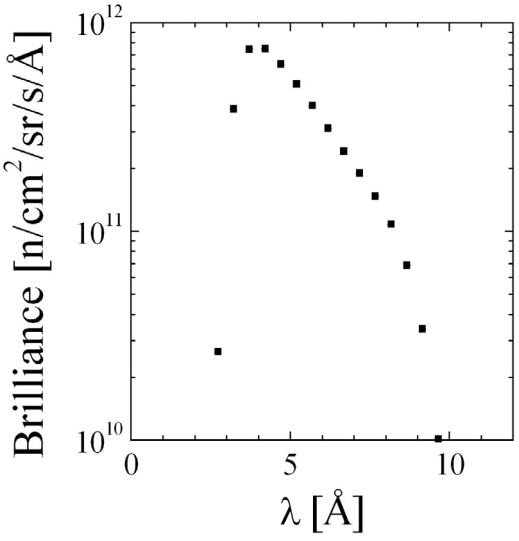


**Fig. 8.** The brilliance at the sample position as a function of wavelength. The dominant wavelength is 4 Å and the decay towards higher wavelengths is due to the Maxwell distribution.

distribution. For the reflectometry mode with 3 beams (using focusing mirrors) and a 2 cm wide and 15 cm long sample, the flux corresponds to approx. $2 \times 10^6$ n/s, $1.5 \times 10^7$ n/s and $5 \times 10^6$ n/s in each of the three beams. The intensities are affected at the higher divergencies because of the finite reflectivities of the neutron guides and mirrors which are modeled in our simulations. However a competing effect is the influence of the relaxed resolution with increasing angle, therefore for 1° the net effect results in highest total intensity. Given these calculated flux values for a typical reflectivity in the range of $10^{-6}$ sufficiently good statistics (±5 to 10%) are collected within about ten minutes or less of exposure time. So already the reflectometry mode is capable of following kinetics on the 10 min time scale reasonably well. A caveat is if the diffuse scattering of the nearby beams blurs the reflectivity signal, more careful analysis and longer counting may be needed. Good GISANS images (1% statistics) will be collected within 10 to 30 mins if the scattering power of the sample is comparable to microemulsions (for 1 mm sample thickness a transmission of 0.554 is obtained, so $\Sigma_{tot} = 6$ cm$^{-1}$). This information is also important for the observable time scales of kinetics.

## 7. Summary

The whole concept of this GISANS instrument is highly promising in terms of intensity and resolution. The reflectometer mode performs similar to the MAgnetic Reflectometer with high Incident Angle (MARIA) [36] at the FRM2 due to the similar average neutron flux ($10^7$ n/cm$^2$/s at 3 mrad collimation) in comparable configurations. Also the incident intensity for the angle 2.5° is highly comparable. MARIA was designed to have 1 × 1 cm $^2$ samples, which are rather small dimensions for GISANS, but still okay for the reflectometry mode. The GISANS mode is also highly promising when compared with the SANS instrument KWS-1 (KWS is the acronym in German for Kleinwinkelstreuung) [49]. KWS-1 has a maximum flux of $10^8$ n/cm$^2$/s with the 2 m collimation and performs well as a GISANS instrument [42]. So we believe that this GISANS instrument at the HBS resides well in the league of high-flux reactor instruments such as at the FRM-2 (MARIA and KWS-1). Thus, top-end research of today can be carried out at this promising instrument.

## Declaration of competing interest

The authors declare that they have no known competing financial interests or personal relationships that could have appeared to influence the work reported in this paper.

## Data availability

No data was used for the research described in the article.

## References

[1] F. Mezei, New perspectives from new generations of neutron sources, C. R. Phys. 8 (7–8) (2007) 909–920.
[2] M. Magán, S. Terrón, K. Thomsen, F. Sordo, J.M. Perlado, F.J. Bermejo, Neutron performance analysis for ESS target proposal, Nucl. Instrum. Methods Phys. Res. A 680 (2012) 61–68.
[3] T. Gutberlet, T. Cronert, T. Brückel, U. Rücker, P. Zakalek, J. Baggemann, Cold moderator systems for compact accelerator-based neutron sources, in: IAEA Technical Meeting on Guidelines for the Establishment and Optimization of Cold Neutron Sources in Research Reactor and Accelerator Facilities (No. FZJ-2018-06581). Streumethoden, 2018.
[4] L. Zanini, K.H. Andersen, K. Batkov, E.B. Klinkby, F. Mezei, T. Schönfeldt, A. Takibayev, Design of the cold and thermal neutron moderators for the European spallation source, Nucl. Instrum. Methods Phys. Res. A 925 (2019) 33–52.
[5] P.K. Willendrup, K. Lefmann, McStas (i): Introduction, use, and basic principles for ray-tracing simulations, J. Neutron Res. 22 (1) (2020) 1–16.
[6] P.K. Willendrup, K. Lefmann, McStas (ii): An overview of components, their use, and advice for user contributions, J. Neutron Res. 23 (1) (2021) 7–27.
[7] K. Lieutenant, J. Voigt, Development of the instrument suite of the HBS, in: International Symposium UCANS9 (No. FZJ-2022-01804). Streumethoden, 2022.
[8] T. Gutberlet, in: T. Brückel (Ed.), Conceptual Design Report-Jülich High Brilliance Neutron Source, HBS, Forschungszentrum Jülich GmbH, Zentralbibliothek, Verlag, 2020.
[9] D.V. Baxter, J.M. Cameron, V.P. Derenchuk, C.M. Lavelle, M.B. Leuschner, M.A. Lone …, W.M. Snow, Status of the low energy neutron source at Indiana university, Nucl. Instrum. Methods Phys. Res. B 241 (1–4) (2005) 209–212.
[10] X. Wang, Q. Xing, C.K. Loong, X. Guan, T. Du, Delivery of 3-MeV proton and neutron beams at CPHS: A status report on accelerator and neutron activities at Tsinghua university, Physics Procedia 60 (2014) 186–192.
[11] M. Furusaka, H. Sato, T. Kamiyama, M. Ohnuma, Y. Kiyanagi, Activity of Hokkaido university neutron source, HUNS, Physics Procedia 60 (2014) 167–174.
[12] T. Kobayashi, S. Ikeda, Y. Otake, Y. Ikeda, N. Hayashizaki, Completion of a new accelerator-driven compact neutron source prototype RANS-II for on-site use, Nucl. Instrum. Methods Phys. Res. A 994 (2021) 165091.
[13] T. Gutberlet, T. Cronert, T. Brückel, U. Rücker, P. Zakalek, J. Baggemann, Cold moderator systems for compact accelerator-based neutron sources, in: IAEA Technical Meeting on Guidelines for the Establishment and Optimization of Cold Neutron Sources in Research Reactor and Accelerator Facilities (No. FZJ-2018-06581). Streumethoden, 2018.

[14] K.H. Andersen, D.N. Argyriou, A.J. Jackson, J. Houston, P.F. Henry, P.P. Deen ., E. Abad, The instrument suite of the European spallation source, Nucl. Instrum. Methods Phys. Res. A 957 (2020) 163402.
[15] S. Mattauch, A. Ioffe, D. Lott, L. Bottyán, J. Daillant, M. Markó ., T. Veres, HERITAGE: the concept of a giant flux neutron reflectometer for the exploration of 3-d structure of free-liquid and solid interfaces in thin films, Nucl. Instrum. Methods Phys. Res. A 841 (2017) 34–46.
[16] A. Glavic, J. Stahn, HEKATE—A novel grazing incidence neutron scattering concept for the European spallation source, Rev. Sci. Instrum. 89 (3) (2018) 035105.
[17] S. Jaksch, D. Martin-Rodriguez, A. Ostermann, J. Jestin, S.D. Pinto, W.G. Bouwman ., H. Frielinghaus, Concept for a time-of-flight small angle neutron scattering instrument at the European spallation source, Nucl. Instrum. Methods Phys. Res. A 762 (2014) 22–30.
[18] S. Jaksch, A. Chennevière, S. Désert, T. Kozielewski, H. Feilbach, P. Lavie ., P. Müller-Buschbaum, Technical specification of the small-angle neutron scattering instrument SKADI at the European spallation source, Appl. Sci. 11 (8) (2021) 3620.
[19] K. Lefmann, K.H. Klenø, J.O. Birk, B.R. Hansen, S.L. Holm, E. Knudsen ., K.H. Andersen, Simulation of a suite of generic long-pulse neutron instruments to optimize the time structure of the European spallation source, Rev. Sci. Instrum. 84 (5) (2013) 055106.
[20] M. Sales, S. Lindahl Holm, K. Lieutenant, K. Lefmann, Powder diffractometers at long-pulsed sources, J. Phys. Soc. Japan 80 (Suppl. B) (2011) SB018.
[21] K.H. Klenø, K. Lieutenant, K.H. Andersen, K. Lefmann, Systematic performance study of common neutron guide geometries, Nucl. Instrum. Methods Phys. Res. A 696 (2012) 75–84.
[22] H. Jacobsen, K. Lieutenant, C. Zendler, K. Lefmann, Bi-spectral extraction through elliptic neutron guides, Nucl. Instrum. Methods Phys. Res. A 717 (2013) 69–76.
[23] H.G. Brühl, T. Baumbach, V. Gottschalch, U. Pietsch, B. Lengeler, Extreme asymmetric X-ray bragg reflection of semiconductor heterostructures near the edge of total external reflection, J. Appl. Crystallogr. 23 (4) (1990) 228–233.
[24] P. Müller-Buschbaum, J.S. Gutmann, M. Stamm, Dewetting of confined polymer films: an X-ray and neutron scattering study, Phys. Chem. Chem. Phys. 1 (17) (1999) 3857–3863.
[25] F. Lipfert, M. Kerscher, S. Mattauch, H. Frielinghaus, Stability of near-surface ordering of bicontinuous microemulsions in external shear-fields, J. Colloid Interface Sci. 534 (2019) 31–36.
[26] P. Müller-Buschbaum, GISAXS and GISANS as metrology technique for understanding the 3D morphology of block copolymer thin films, Eur. Polym. J. 81 (2016) 470–493.
[27] A. Perrichon, A. Devishvili, K. Komander, G.K. Pálsson, A. Vorobiev, R. Lavén ., M. Wolff, Resonant enhancement of grazing incidence neutron scattering for the characterization of thin films, Phys. Rev. B 103 (23) (2021) 235423.
[28] S. Nouhi, M.S. Hellsing, V. Kapaklis, A.R. Rennie, Grazing-incidence small-angle neutron scattering from structures below an interface, J. Appl. Crystallogr. 50 (4) (2017) 1066–1074.
[29] T. Kyrey, M. Ganeva, J. Witte, A. Feoktystov, S. Wellert, O. Holderer, Grazing incidence small-angle neutron scattering: Background determination and optimization for soft matter samples, Appl. Sci. 11 (7) (2021) 3085.
[30] R. Kampmann, M. Haese-Seiller, V. Kudryashov, B. Nickel, C. Daniel, W. Fenzl ., J. Rädler, Horizontal ToF-neutron reflectometer REFSANS at FRM-II Munich/Germany: first tests and status, Physica B 385 (2006) 1161–1163.
[31] H. Frielinghaus, M. Gvaramia, G. Mangiapia, S. Jaksch, M. Ganeva, A. Koutsioubas ., O. Holderer, New tools for grazing incidence neutron scattering experiments open perspectives to study nano-scale tribology mechanisms, Nucl. Instrum. Methods Phys. Res. A 871 (2017) 72–76.
[32] B.J. Kirby, P.A. Kienzle, B.B. Maranville, N.F. Berk, J. Krycka, F. Heinrich, C.F. Majkrzak, Phase-sensitive specular neutron reflectometry for imaging the nanometer scale composition depth profile of thin-film materials, Curr. Opin. Colloid Interface Sci. 17 (1) (2012) 44–53.
[33] M. Wolff, A. Devishvili, J.A. Dura, F.A. Adlmann, B. Kitchen, G.K. Pálsson ., B.P. Toperverg, Nuclear spin incoherent neutron scattering from quantum well resonators, Phys. Rev. Lett. 123 (1) (2019) 016101.
[34] B. Wiedemann, A. Chacon, S.L. Zhang, Y. Khaydukov, T. Hesjedal, O. Soltwedel ., P. Böni, Reciprocal space mapping of magnetic order in thick epitaxial MnSi films, 2017, arXiv preprint arXiv:1710.00544.
[35] Y.V. Nikitenko, A.V. Petrenko, N.A. Gundorin, Y.M. Gledenov, V.L. Aksenov, Isotope-identifying neutron reflectometry, Crystallogr. Rep. 60 (4) (2015) 466–479.
[36] S. Mattauch, A. Koutsioubas, U. Rücker, D. Korolkov, V. Fracassi, J. Daemen ., T. Bruckel, The high-intensity reflectometer of the Jülich centre for neutron science: MARIA, J. Appl. Crystallogr. 51 (3) (2018) 646–654.
[37] P. Müller-Buschbaum, Grazing incidence small-angle neutron scattering: challenges and possibilities, Polym. J. 45 (1) (2013) 34–42.
[38] A. Hexemer, P. Müller-Buschbaum, Advanced grazing-incidence techniques for modern soft-matter materials analysis, IUCrJ 2 (1) (2015) 106–125.
[39] M. Wolff, Grazing incidence scattering, in: EPJ Web of Conferences Vol. 188, EDP Sciences, 2018, p. 04002.
[40] S. Jaksch, T. Gutberlet, P. Müller-Buschbaum, Grazing-incidence scattering—status and perspectives in soft matter and biophysics, Curr. Opin. Colloid Interface Sci. 42 (2019) 73–86.
[41] S. Jaksch, F. Lipfert, A. Koutsioubas, S. Mattauch, O. Holderer, O. Ivanova ., B. Nickel, Influence of ibuprofen on phospholipid membranes, Phys. Rev. E 91 (2) (2015) 022716.
[42] S. Ueda, S. Koizumi, A. Ohira, S. Kuroda, H. Frielinghaus, Grazing-incident neutron scattering to access catalyst for polymer electrolyte fuel cell, Physica B 551 (2018) 309–314.
[43] V. Pipich, M. Dickmann, H. Frielinghaus, R. Kasher, C. Hugenschmidt, W. Petry ., D. Schwahn, Morphology of thin film composite membranes explored by small-angle neutron scattering and positron-annihilation lifetime spectroscopy, Membranes 10 (3) (2020) 48.
[44] R. Gilles, V. Zinth, S. Seidlmayer, N. Paul, M. Hofmann, J. Hattendorff ., J.F. Moulin, Why neutrons for li ion battery research? in: ECS Meeting Abstracts (No. 5, p. 265), IOP Publishing, 2014.
[45] B. Wiedemann, A. Chacon, S.L. Zhang, Y. Khaydukov, T. Hesjedal, O. Soltwedel ., P. Böni, Reciprocal space mapping of magnetic order in thick epitaxial MnSi films, 2017, arXiv preprint arXiv:1710.00544.
[46] L. Song, W. Wang, V. Körstgens, D.M. González, Y. Yao, N.K. Minar ., P. Müller-Buschbaum, Spray deposition of titania films with incorporated crystalline nanoparticles for all-solid-state dye-sensitized solar cells using P3HT, Adv. Funct. Mater. 26 (10) (2016) 1498–1506.
[47] C.J. Brett, N. Mittal, W. Ohm, M. Gensch, L.P. Kreuzer, V. Körstgens ., S.V. Roth, Water-induced structural rearrangements on the nanoscale in ultrathin nanocellulose films, Macromolecules 52 (12) (2019) 4721–4728.
[48] M. Zhernenkov, M. Dubey, B. Toperverg, J. Majewski, M. Fitzsimmons, Lipid domains in supported SM-chol membranes measured by GISANS, in: APS March Meeting Abstracts (Vol. 2011, pp. B40-012), 2011.
[49] A.V. Feoktystov, H. Frielinghaus, Z. Di, S. Jaksch, V. Pipich, M.S. Appavou ., T. Brückel, KWS-1 high-resolution small-angle neutron scattering instrument at JCNS: current state, J. Appl. Crystallogr. 48 (1) (2015) 61–70.
[50] M. Kerscher, P. Busch, S. Mattauch, H. Frielinghaus, D. Richter, M. Belushkin, G. Gompper, Near-surface structure of a bicontinuous microemulsion with a transition region, Phys. Rev. E 83 (3) (2011) 030401.
[51] M. Ballauff, SAXS and SANS studies of polymer colloids, Curr. Opin. Colloid Interface Sci. 6 (2) (2001) 132–139.
[52] B. Hammouda, SANS from polymers—review of the recent literature, J. Macromol. Sci. C: Polym. Rev. 50 (1) (2010) 14–39.
[53] M. Kerscher, F. Lipfert, H. Frielinghaus, Exploring hidden local ordering in microemulsions with a weak directive second order parameter, Chem. Afr. 3 (3) (2020) 703–709.
[54] https://www.rri.kyoto-u.ac.jp/en/facilities/nmfs (last access Dec 15 2022).
[55] C. Schanzer, M. Schneider, P. Böni, Neutron optics: Towards applications for hot neutrons, in: Journal of Physics: Conference Series (Vol. 746, No. 1, p. 012024), IOP Publishing, 2016.
[56] S.M. Choi, J. Barker, C.J. Glinka, Y.T. Cheng, P.L. Gammel, Focusing cold neutrons with multiple biconcave lenses for small-angle neutron scattering, J. Appl. Crystallogr. 33 (3) (2000) 793–796.